Received: 30 October 2017 | Revised: 14 June 2018 | Accepted: 3 September 2018

DOI: 10.1002/nag.2858

RESEARCH ARTICLE

WILEY

On the linear elastic responses of the 2D bonded discrete element model

Gao-Feng Zhao[1] | Qiuyue Yin[1] | Adrian R. Russell[2] | Yingchun Li[3,4] | Wei Wu[3] | Qin Li[1]

[1]State Key Laboratory of Hydraulic Engineering Simulation and Safety, School of Civil Engineering, Tianjin University, Tianjin 300072, China

[2]Centre for Infrastructure Engineering and Safety, School of Civil and Environmental Engineering, The University of New South Wales, Sydney, NSW 2052, Australia

[3]School of Civil and Environmental Engineering, Nanyang Technological University, 639798, Singapore

[4]School of Civil and Hydraulic Engineering, Dalian University of Technology, Dalian 116024, China

Correspondence
Gao-Feng Zhao, State Key Laboratory of Hydraulic Engineering Simulation and Safety, School of Civil Engineering, Tianjin University, Tianjin 300072, China.
Email: gaofeng.zhao@tju.edu.cn

Funding information
National Natural Science Foundation of China, Grant/Award Number: 1177020290

Summary

The bonded discrete element model (DEM) is a numerical tool that is becoming widely used when studying fracturing, fragmentation, and failure of solids in various disciplines. However, its abilities to solve elastic problems are usually overlooked. In this work, the main features of the 2D bonded DEM which influence Poisson's ratio and Young's modulus, and accuracy when solving elastic boundary value problems, are investigated. Outputs of numerical simulations using the 2D bonded DEM, the finite element method, a hyper elasticity analysis, and the distinct lattice spring model (DLSM) are compared in the investigation. It is shown that a shear interaction (local) factor and a geometric (global) factor are two essential elements for the 2D bonded DEM to reproduce a full range of Poisson's ratios. It is also found that the 2D bonded DEM might be unable to reproduce the correct displacements for elastic boundary value problems when the represented Poisson's ratio is close to 0.5 or the long-range interaction is considered. In addition, an analytical relationship between the shear stiffness ratio and the Poisson's ratio, derived from a hyper elasticity analysis and applicable to discontinuum-based models, provides good agreement with outputs from the 2D bonded DEM and DLSM. Finally, it is shown that the selection of elastic parameters used the 2D bonded DEM has a significant effect on fracturing and fragment patterns of solids.

KEYWORDS

discrete element model, fracturing, fragmentation, hyper elasticity analysis, Poisson's ratio

1 | INTRODUCTION

The discrete element model (DEM),[1] developed to model granular materials,[2] was extended by Potyondy and Cundall[3] through the introduction of a particle bonding scheme so problems involving rock and other solids can be modeled. The bonded DEM has become a widely used numerical tool. Examples of its many applications include the cracking of composite materials,[4] bending test of concrete beam,[5] crack propagation and coalescence of rock,[6,7] fragmentation of rock during tunnel boring,[8] stability analysis of retaining walls,[9] failure of jointed rock slopes,[10] hydraulic fracturing of reservoirs,[11] and development of contractional fault-related folds.[12] Its most attractive feature is the ability to model complex macroscopic phenomena, eg, fracturing and fragmentation, which are difficult to model using traditional continuum-based approaches. Results of the bonded DEM are usually very close to those of physical experiments. For example, the three-dimensional failure envelope for rock recovered from the bonded DEM agrees well the experimental observations,[13] including strengths and crack patterns.[6,7] Previous studies have advocated the use of the bonded

DEM in problems involving fracturing, fragmentation and failure of solids. However, its abilities to solve elastic problems have not been explored in detail.

The Poisson's ratio and Young's modulus control the elastic responses of solids. For continuum-based numerical methods, eg, the finite element method (FEM), they are inputs, whereas, they are outputs for discontinuum-based models such as the bonded DEM. For example, direct input elastic parameters of the bonded DEM are usually the normal stiffness and shear stiffness. Difficulty on representing a full range of Poisson's ratios is an intrinsic problem of many discontinuum-based models, eg, the lattice spring model (LSM),[14] the lattice solid model (LSM),[15] and the virtual internal bond model.[16] Continuous efforts have been conducted to resolve this limitation, giving rise to the beam element model by Lilliu and van Mier,[17] the multibody shear spring by Zhao et al,[18] the nonlocal potential by Chen et al,[19] the modified Stillinger-Weber potential by Zhang et al,[20,21] and the fourth-dimensional interaction by Zhao.[22] For the bonded DEM, a full range of the Poisson's ratios can be achieved by adjusting the stiffness ratio of the shear spring and the normal spring (shear stiffness ratio) in the bonds.[23,24] However, attention has not been given to the influence of particle contact geometry in the relationship between Poisson's ratio and shear stiffness ratio. Most attention has been given to idealized or regular particle packings,[25] overlooking the influence of randomness which may exist in some packings. Shear stiffness is often ignored in order to simplify an analysis[26] thus restricting the Poisson's ratio of the material to be 1/3. Also, the rotational degree of freedom (DOF) of particles causes the bonded DEM to behave more consistently with the laws of micro-polar elasticity than classical elasticity, yet this is not well understood. Furthermore, the number of input parameters of the bonded DEM (eg, the bond normal stiffness, the shear stiffness, and bending stiffness) are usually inconsistent with the macroscopic parameters (eg, the Young's modulus and Poisson's ratio). It is the culmination of these factors which means that using the bonded DEM in rigorous elastic analysis of wide applicability is very challenging.

In this work, the abilities of the 2D bonded DEM to solve elastic problems are comprehensively investigated. To make consistency between the number of micro and macro elastic parameters, a sub-spring scheme is adopted. The elastic parameters recovered from the 2D bonded DEM are compared with those recovered from the FEM, a hyper elasticity analysis, and the distinct lattice spring model (DLSM). The effect of particle rotation, particle packing geometry, and model dimension is also studied by comparing outputs from these varied numerical and analytical methods.

2 | METHODS

To study abilities of the 2D bonded DEM to solve elastic problems, a modified bonded DEM is used to maintain consistency between micro and macro elastic parameters. Outputs are compared with those obtained using the FEM for boundary value problems, as well as hyper elasticity and DLSM when investigating influences of particle rotation, homogeneity of deformation, and the model dimension. The different numerical methods are briefly introduced in this section, excluding the FEM as it is a well-known and well documented method.

2.1 | The 2D bonded DEM

The basic principle of the 2D bonded DEM is illustrated in Figure 1. The target domain is discretized into a group of particles, which are bonded by spring. The deformation and failure of the solid are represented by the deformation

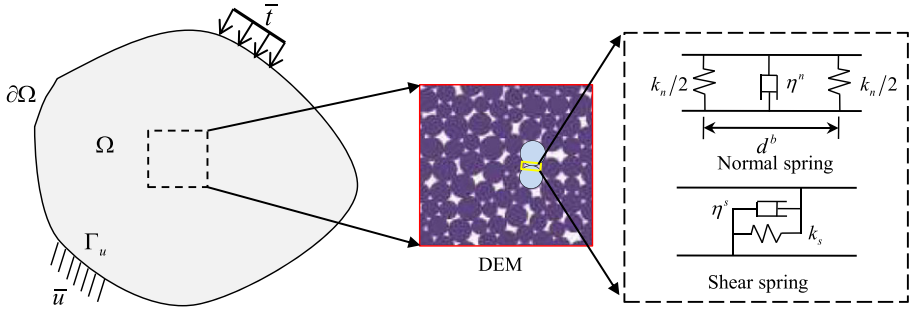

FIGURE 1 The basic principle of the bonded DEM for solid mechanical problems [Colour figure can be viewed at wileyonlinelibrary.com]

and failure of the spring bonds. Bending springs are usually employed in the bonded DEM to enable moment transfer between particles, which results in an inconsistency between the number of micro and macro elastic parameters. In this work, inspired by the multiple contact point formulation,[27] a two sub-normal spring configuration is used (see Figure 1) for describing the normal interaction between two particles. The moment transfer between two particles can be considered by using a dimensionless coefficient (*dWR*) to introduce a distance between two sub-normal springs (see Figure 1) as

$$d_b = dWR \times \min\left(R_i, R_j\right) \tag{1}$$

where d_b is the distance between two sub-springs, R_i and R_j are the radii of the two linked particles, and *dWR* is a dimensionless coefficient which can be assigned a value between 0 and 1. A *dWR* equal to zero corresponds to the normal spring adopted by the classical DEM. The larger the *dWR*, the stronger the bending stiffness between particles. Let the relative angular velocity of particle i with respect to particle j be

$$\dot{\theta}_{ij} = \dot{\theta}_j - \dot{\theta}_i \tag{2}$$

in which $\dot{\theta}_i$ and $\dot{\theta}_j$ are angular velocities of particles i and j, respectively. The forces of the sub-springs induced by the particle rotation are given as

$$\Delta F_n^{\Theta} = \pm\frac{1}{4}\dot{\theta}_{ij}\Delta t d_b k_n \tag{3}$$

where Δt is the time step and k_n is the normal stiffness of the bond. The moment between particles induced from particle rotations can be expressed as

$$\Delta M_{ij}^{\Theta} = \frac{1}{4}\dot{\theta}_{ij}\Delta t d_b^2 k_n \tag{4}$$

The angular velocity-induced normal force between two particles is zero due to the forces of two sub-springs canceling out each other (see Equation 3). The incremental normal force between two particles is calculated as

$$\Delta F_n = k_n v_n \Delta t \tag{5}$$

in which the normal velocity v_n of the contact is obtained as

$$v_n = \left(\dot{x}_j - \dot{x}_i\right)n_x + \left(\dot{y}_j - \dot{y}_i\right)n_y \tag{6}$$

where $\dot{x}_i$ and $\dot{x}_j$ are the particle velocities in each direction. n_x and n_y are the normal components of the contact which are calculated as

$$n_x = \frac{x_j - x_i}{\sqrt{\left(x_j - x_i\right)^2 + \left(y_j - y_i\right)^2}} \tag{7}$$

$$n_y = \frac{y_j - y_i}{\sqrt{\left(x_j - x_i\right)^2 + \left(y_j - y_i\right)^2}}. \tag{8}$$

Thus, the incremental normal force of each sub-spring can be written as

$$\Delta \widetilde{F}_n^{\Theta} = \frac{1}{2}k_n v_n \Delta t \pm \frac{1}{4}\dot{\theta}_{ij}\Delta t d_b k_n \tag{9}$$

The shear force increment is given as

$$\Delta F_s = k_s v_s \Delta t \tag{10}$$

where k_s is the shear stiffness. v_s is the relative shear velocity which can be obtained as

$$v_s = -\left(\dot{x}_j - \dot{x}_i\right)n_y + \left(\dot{y}_j - \dot{y}_i\right)n_x - \dot{\theta}_i R_i - \dot{\theta}_j R_j. \tag{11}$$

The contact forces are obtained from an integration of the incremental forces. External forces of a given particle are obtained from a sum operation over all the contacts linked to the particle.

The long-range interaction between particles was incorporated in to the bonded DEM to prevent an unreasonably low ratio between tensile and compressive strengths from being recovered.[28] In this work, to consider the long-range interaction, the criterion of forming bonds between particles is given as

$$\sqrt{\left(x_j - x_i\right)^2 + \left(y_j - y_i\right)^2} - R_i - R_j < dGap \tag{12}$$

where x, y, and R are the coordinates and radius of the particle with index of i or j; $dGap$ is the threshold value for formation of bonds. For a given particle model, varying numbers of bonds can be formed by using different threshold values. In this work, we define as average contact number (CN) as the total number of spring bonds divided by the total number of particles. During a bonded DEM computation, the modified Mohr-Coulomb criterion is applied to the bonds. When either sub-bond breaks, the bond turns into a contact pair as in the classical DEM. To apply boundary conditions, wall elements are also implemented. Details on equations and implementation of the DEM can be found in the work of Zhao.[29] The source code used in this work is accessible publicly at www.dembox.org.

2.2 | Hyper elasticity analysis

Hyper elasticity analyses are commonly used by researchers, eg, Gao and Klein,[16] Zhang and Ge,[30] and Zhao,[22] to study elastic responses of discontinuum-based models. In this work, outputs from hyper elasticity analyses are compared with elastic responses of the bonded DEM. As shown in Figure 2, consider that a deformation state ε_{ij} is imposed on a cube with side length of L, which is linked with spring bonds that consist of normal and shear springs. Since there is no relative rotation between particles, it is not necessary to consider the moment transfer between particles. The energy stored in the 3D bonded DEM is the sum of energy stored in these spring bonds. Because translation of the spring bonds will not influence their deformation energy, the distribution of bonds in the cube can be equivalent to a semi sphere distribution as shown in Figure 2B. Under the spherical coordinate, the strain energy stored in the normal spring is

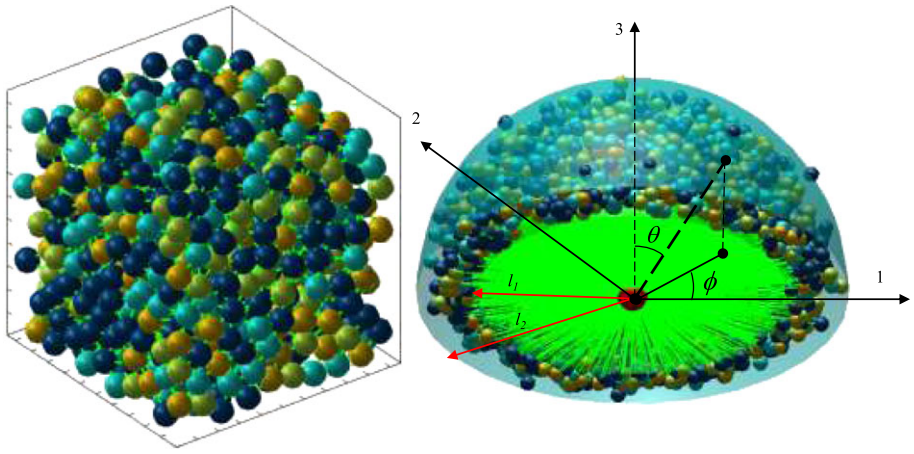

FIGURE 2 Three-dimensional bonded particle model and its energy equivalent form: A, the original model under Cartesian coordinate system; B, equivalent bond distribution under the spherical coordinate system (formed by translate operations over the original bonds) [Colour figure can be viewed at wileyonlinelibrary.com]

$$U_n = \frac{1}{2}k_n l^2 \left(\xi_i \varepsilon_{ij} \xi_j\right)^2 \tag{13}$$

where k_n is the stiffness of the normal spring, l is the initial length, and $\xi = (\sin\theta\cos\phi, \sin\theta\sin\phi, \cos\theta)$ is the direction vector of the bond expressed in terms of spherical coordinates. The strain energy stored in the shear spring is obtained as

$$U_s = \frac{1}{2}k_s u_s^2 \tag{14}$$

where u_s and k_s are the displacement and stiffness of the shear spring, respectively. Based on tensor and vector operation, the above equation can be further written as

$$U_s = \frac{1}{2}k_s l^2 \left(\varepsilon_{kl}\xi_l - \xi_i \varepsilon_{ij}\xi_j\xi_k\right)\left(\varepsilon_{km}\xi_m - \xi_n \varepsilon_{nm}\xi_m\xi_k\right). \tag{15}$$

Then, the total energy stored per unit volume is expressed as

$$\Phi = \frac{\sum U_n + \sum U_s}{L^3}. \tag{16}$$

The elastic tensor of the particle model can be obtained through the hyper-elastic theory and be expressed as

$$c_{ijnm} = \frac{\partial^2 \Pi}{\partial \varepsilon_{ij}\partial \varepsilon_{nm}} = \sum \frac{l^2\left(k_n \xi_i\xi_j\xi_n\xi_m + k_s\left(\delta_{in}\xi_j\xi_m - \xi_i\xi_j\xi_n\xi_m\right)\right)}{L^3}. \tag{17}$$

When the number of spring bonds in the cube is sufficiently large, the above equation can be written as

$$c_{ijnm} = \frac{1}{L^3}\int_{l_1}^{l_2}\int_0^{2\pi}\int_0^{\pi} l^2\left(k_n \xi_i\xi_j\xi_n\xi_m + k_s\left(\delta_{in}\xi_j\xi_m - \xi_i\xi_j\xi_n\xi_m\right)\right) D(l,\theta,\phi)\sin(\theta) d\,\theta d\,\phi dl \tag{18}$$

where $D(l,\theta,\phi)\sin(\theta)d\theta d\phi dl$ is the number of contacts per unit volume in the undeformed particle model with bond length between $(l, l+dl)$ and bond orientation between $(\theta, \theta+d\theta)$ and $(\phi, \phi+d\phi)$. The tensor of linear elasticity c_{ijnm} can be written in the matrix form as

$$\Omega = \begin{bmatrix} C_{1111} & C_{1122} & C_{1133} & \frac{1}{2}(C_{1112}+C_{1121}) & \frac{1}{2}(C_{1132}+C_{1123}) & \frac{1}{2}(C_{1113}+C_{1131}) \\ C_{2211} & C_{2222} & C_{2233} & \frac{1}{2}(C_{2212}+C_{2221}) & \frac{1}{2}(C_{2232}+C_{2223}) & \frac{1}{2}(C_{2213}+C_{2231}) \\ C_{3311} & C_{3322} & C_{3333} & \frac{1}{2}(C_{3312}+C_{3321}) & \frac{1}{2}(C_{3332}+C_{3323}) & \frac{1}{2}(C_{3313}+C_{3331}) \\ C_{1211} & C_{1222} & C_{1233} & \frac{1}{2}(C_{1212}+C_{1221}) & \frac{1}{2}(C_{1232}+C_{1223}) & \frac{1}{2}(C_{1213}+C_{1231}) \\ C_{2311} & C_{2322} & C_{2333} & \frac{1}{2}(C_{2312}+C_{2321}) & \frac{1}{2}(C_{2332}+C_{2323}) & \frac{1}{2}(C_{2313}+C_{2331}) \\ C_{1311} & C_{1322} & C_{1333} & \frac{1}{2}(C_{1312}+C_{1321}) & \frac{1}{2}(C_{1332}+C_{1323}) & \frac{1}{2}(C_{1313}+C_{1331}) \end{bmatrix}. \tag{19}$$

For an isotropic material, when the bonds are distributed uniformly in each direction, the corresponding elastic matrix of the 3D bonded DEM can be written as

$$\Omega = \frac{\int_{l_1}^{l_2} l^2 N(l) dl}{15L^3} \begin{bmatrix} 3k_n + 2k_s & k_n - k_s & k_n - k_s & 0 & 0 & 0 \\ & 3k_n + k_s & k_n - k_s & 0 & 0 & 0 \\ & & 3k_n + 2k_s & 0 & 0 & 0 \\ & & & k_n + 1.5k_s & 0 & 0 \\ & \text{symmetry} & & & k_n + 1.5k_s & 0 \\ & & & & & k_n + 1.5k_s \end{bmatrix}. \tag{20}$$

Let $\alpha^{3D} = \int_{l_1}^{l_2} l^2 N(l) dl / L^3$, then the relationship between the spring parameters k_n, k_s and the macro material constants, ie, the Young's modulus E and the Poisson ratio v are obtained as

$$k_n = \frac{3E}{\alpha^{3D}(1-2v)} \tag{21}$$

$$k_s = \frac{3(1-4v)E}{\alpha^{3D}(1+v)(1-2v)}. \tag{22}$$

Then, an analytical relationship between the shear stiffness ratio and the Poisson's ratio is obtained as

$$v = \frac{1 - k_s/k_n}{4 + k_s/k_n}. \tag{23}$$

Equation 23 provides an analytical solution for the Poisson's ratio of the 3D bonded DEM, whose applicability will be further verified in this work.

2.3 | The distinct lattice spring model (DLSM)

The uniform deformation assumption adopted in the hyper elasticity analysis can be further released in the DLSM which is a 3D approach. DLSM only considers three translational DOFs for each particle and is free of the rotational DOFs. Therefore, it is a good candidate to be used as a reference for the influence of particle rotation. The DLSM adopts a similar solving procedure as the bonded DEM. The major difference is the equations used to calculate the interaction between particles. Here, only a brief description of the DLSM is given to highlight the main difference. Comprehensive details of the DLSM can be found in the work of Zhao et al.[18] Two types of springs are used in the DLSM. The first one is the normal spring, which can be represented as

$$\mathbf{F}_{ij}^n = k_n \mathbf{u}_{ij}^n \tag{24}$$

where k_n is the stiffness of the normal spring and $\mathbf{u}_{ij}^n$ represents the vector of the normal displacement which is given as

$$\mathbf{u}_{ij}^n = \left(\left(\mathbf{u}_j - \mathbf{u}_i\right)\mathbf{n}\right)\mathbf{n} \tag{25}$$

where $\mathbf{u}$ is the particle displacement and $\mathbf{n}$ is the normal vector point from particle i to particle j.

In the DLSM, the local strain of a particle is calculated using a least square method over the displacements of a cloud of particles linked to the particle. The local strain of the shear spring is obtained as

$$[\varepsilon]_{bond} = \frac{[\varepsilon]_i + [\varepsilon]_j}{2} \tag{26}$$

in which $[\varepsilon]_i$ and $[\varepsilon]_j$ represent the local strains for the two particles connected by the spring bond. Then, the shear displacement of the bond is obtained as

$$\widehat{\mathbf{u}}_{ij}^s = [\varepsilon]_{bond} \cdot \mathbf{n} l - \left(\left([\varepsilon]_{bond} \cdot \mathbf{n} l\right) \cdot \mathbf{n}\right)\mathbf{n} \tag{27}$$

where l is the distance between the two particles.

Hence, the shear force is calculated as

$$\mathbf{F}_{ij}^{s} = k_s \widehat{\mathbf{u}}_{ij}^{s} \tag{28}$$

where k_s is the stiffness of the shear spring.

3 | NUMERICAL MODELING AND DISCUSSION

In this section, the elastic responses of the 2D bonded DEM are investigated and compared with those recovered using the other methods.

3.1 | Triangle-packed DEM

The regular triangle-packed model provides a good reference to investigate some fundamental aspects of the 2D bonded DEM, especially the shear stiffness ratio. For all simulations, the local damping coefficient of 0.5 is adopted to obtain the static solution.

3.1.1 | A simple boundary value problem: The uniaxial compression test

Figure 3 shows the computational model used to extract the Poisson's ratio and Young's modulus. Two configurations of the spring bonds are formed by setting different threshold values for the bond formation. The first computational model is a classical triangle lattice in which two particles form a contact when they touch each other. The CN of the particle model shown in Figure 3 is 5.60 (the number particles along the bottom line is $N = 20$). CN differs from coordination number (which would be 6 for this packing) as no weighting correction is given to particles and bonds at the model boundaries in its calculation. The second model considers the long-range interaction, where the second layer of neighbors is also interacted with each other (see Figure 3B). The model can be characterized by CN = 16.2 and $N = 20$. The particles of these models are arranged in a way to achieve symmetry about the vertical centre line. Two walls are used to apply the boundary conditions: the bottom one is fixed during the simulation, while, the top wall is moved at the constant velocity of 0.001 m/s to impose a deformation for the specimen to mimic a uniaxial compression loading. The specimen size can be characterized by the number of particles on the bottom line N which is used to refer the resolution of the computational model. The computational models shown in Figure 3 are two typical particle models when $N = 20$. The particle size is 20 m, and the dimension of the specimen can be expressed using N and the particle radius (see Figure 3). During the simulation, the reaction force of the top wall and the displacements at the four measuring points

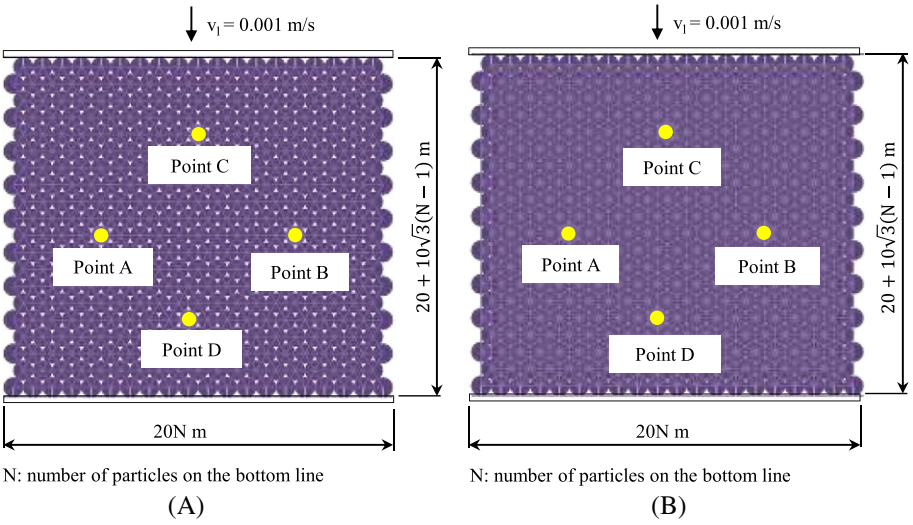

FIGURE 3 Triangle-packed DEMs for the UCS test to extract the Poisson's ratio and elastic modulus: A, CN = 5.60; B, CN = 16.12 [Colour figure can be viewed at wileyonlinelibrary.com]

(A, B, C, and D) (see Figure 3) are recorded. The corresponding Poisson's ratio and Young's modulus are obtained using the following equations:

$$v(t) = \frac{\left(u_B^x(t) - u_A^x(t)\right)/\left(x_B^0 - x_A^0\right)}{\left(u_C^y(t) - u_D^y(t)\right)/\left(y_C^0 - y_D^0\right)} \tag{29}$$

$$E(t) = \frac{F(t)/W}{U(t)/H} \tag{30}$$

where $v(t)$ and $E(t)$ are the Poisson's ratio and Young's modulus at time t; $u_A^x(t)$ and $u_B^x(t)$ are the recorded displacements in the x direction at measuring points A and B; $u_C^y(t)$ and $u_D^y(t)$ are particle displacements in the y direction at measuring points C and D; x_A^0 and x_B^0 are the initial x coordinates of the measuring points A and B; y_C^0 and y_D^0 are the initial y coordinates of the measuring points C and D; $F(t)$ and $U(t)$ are the recorded displacement and force of the top wall during simulation; and W and H are the width and height of the specimen. During simulation, v (t) and E (t) will be converged into stable values which were recorded as the measured elastic constants for the bonded DEM.

The model's resolution (that is the model size compared with particle size) may influence the results. A parametric analysis is conducted, specifically on the influence of N on the results. It is found that resolution influences are negligible when N is equal to 20 or more. In the 2D bonded DEM, when $dWR = 0$, it means the relative rotation between two particles is not constrained, and there is no moment transfer between them. When dWR is larger than zero, the relative rotation is constrained, and the moment can be transferred between two particles. In our numerical simulation, no apparent difference is observed when dWR was changed to 0.0, 0.2, or 0.8.

Figure 4 shows the influence of shear stiffness ratio on the Poisson's ratio and Young's modulus of the triangle-packed DEM. The Young's modulus is scaled with that of the bonded DEM when shear stiffness ratio is zero. An upper limit for the Poisson's ratio of 1/3, the limit value of LSM, was found for the triangle-packed model irrespective of whether long-range interactions are considered or not. As shown in Figure 4, the Poisson's ratio decreases when the shear stiffness ratio increases. The reason might be that the lateral movement of the bonded particle model is further constrained due to the increase of the shear stiffness. For the Young's modulus, the increase of shear stiffness ratio causes an increase. For the model with CN = 16.12, the increase of modulus by increasing the shear stiffness ratio is less than that for the model with CN = 5.60. In the following, these models will be further used to investigate the ability of the bonded DEM on solving elastic problems with complex deformation fields.

3.1.2 | An elastic problem with a complex deformation field

A high-resolution model is used, having $N = 100$. The top wall, which does not extend across the entire top boundary (Figure 5), is pushed in to the model at a constant velocity to achieve a vertical displacement of 0.0896 m. The

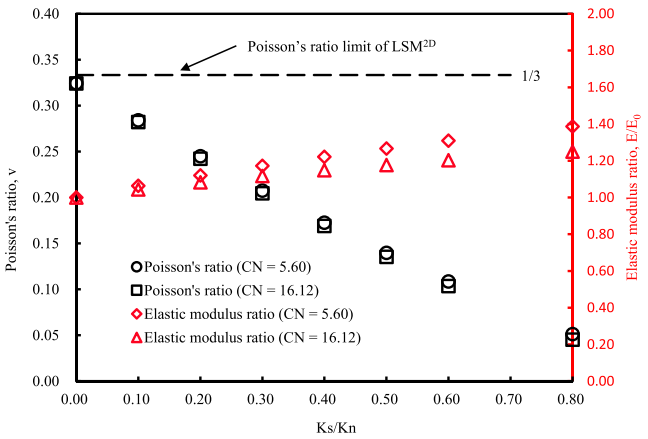

FIGURE 4 Influence of the shear stiffness ratio on the Poisson's ratio and elastic modulus ratio of the triangle-packed DEM [Colour figure can be viewed at wileyonlinelibrary.com]

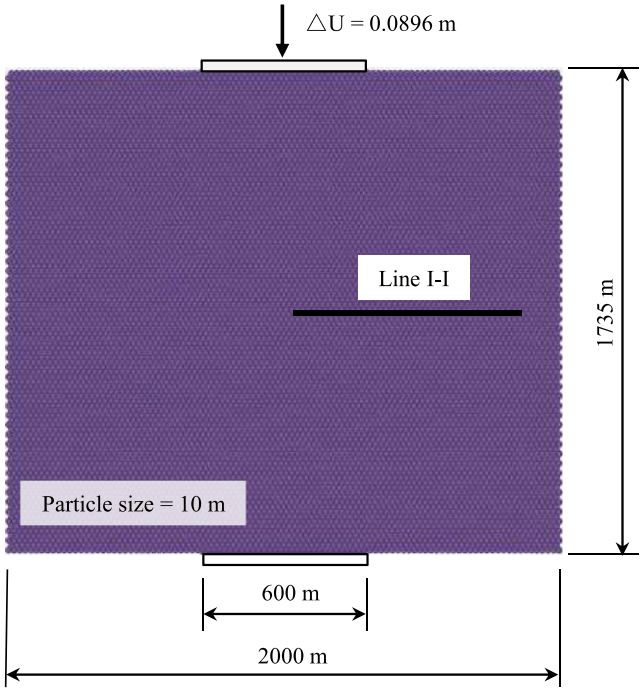

FIGURE 5 Numerical configuration of the triangle-packed DEM for a boundary-value problem [Colour figure can be viewed at wileyonlinelibrary.com]

loading velocity is then turned to zero until a stable solution is achieved. For this elastic problem, the deformation field is controlled by the Poisson's ratio. The plane stress FEM was used as the reference solution. The element size in the FEM was taken as 20 m to maintain a resolution of the same order as the DEM. Figure 6 shows the comparison between displacements obtained at the same measure lines of the bonded DEM and the plane stress FEM. The bonded DEM with CN = 5.92 yields the same results as the FEM. However, it is found that when *CN* = 17.62, the bonded DEM cannot give the correct elastic deformation results. In the 2D bond DEM, long-rang interaction (large CN) was adopted to achieve higher ratio of compressive strength to tensile strength.[28] However, from our simulation results, the 2D bonded DEM with long-range interaction (large CN) might face difficulties in representing the elastic deformation field correctly. Therefore, caution must be taken when the long-range interaction is adopted in the 2D bonded DEM.

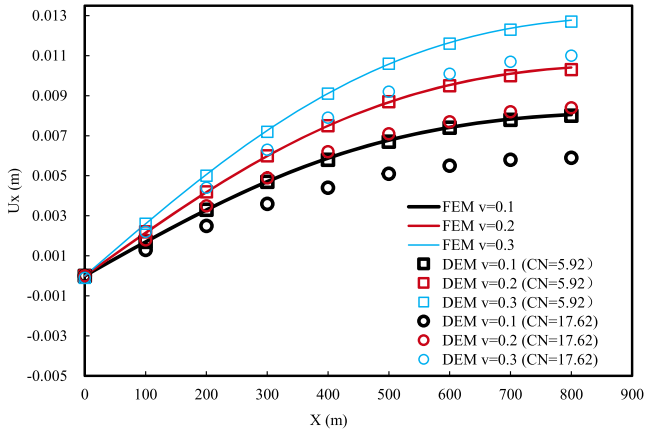

FIGURE 6 Quantitative comparison of displacements predicted by the FEM and the triangle-packed DEM for the boundary value problem [Colour figure can be viewed at wileyonlinelibrary.com]

3.2 | Random-packed DEM

3.2.1 | A simple boundary value problem: The uniaxial compression test

Figure 7 shows the random-packed DEM, in which the particle sizes are polydisperse and have an average size of 15.83 m. Models with different CNs can be generated by setting different threshold values for the bond formation. The same procedures for extracting the Poisson's ratio and Young's modulus for the triangle packed DEM are adopted here. The results on the Poisson's ratio of the random-packed DEM are shown in Figure 8. It shows that the reproduced Poisson's ratio of the 2D bonded DEM can even equal to 1. Because under plan strain condition, the incompressible material ($\nu = 0.5$) in 2D will have an apparent Poisson's ratio of 1. When the CN is close to the triangle-packed DEM, the represented Poisson's ratio will close to these triangle-packed models (see Figure 8). As shown in Figure 8, the increase of shear stiffness ratio will decrease the Poisson's ratio. When the shear stiffness ratio is large enough, a

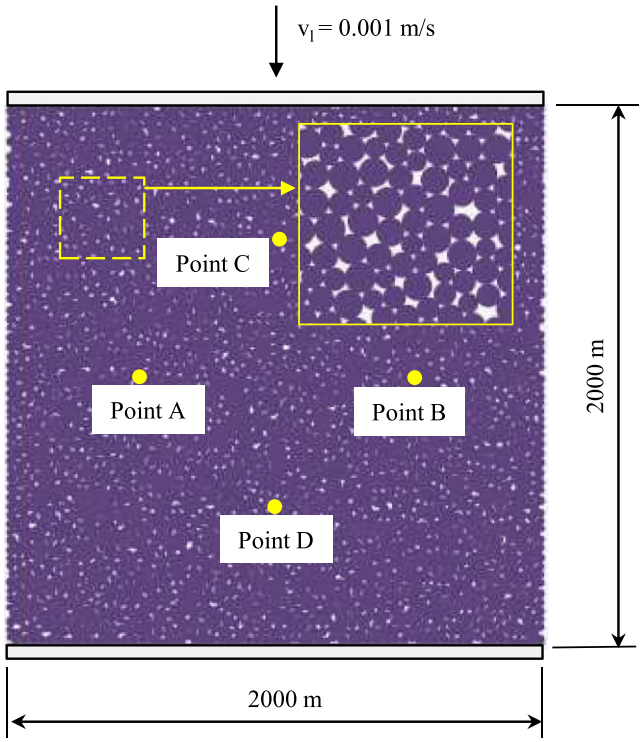

FIGURE 7 The random-packed DEM for the UCS test [Colour figure can be viewed at wileyonlinelibrary.com]

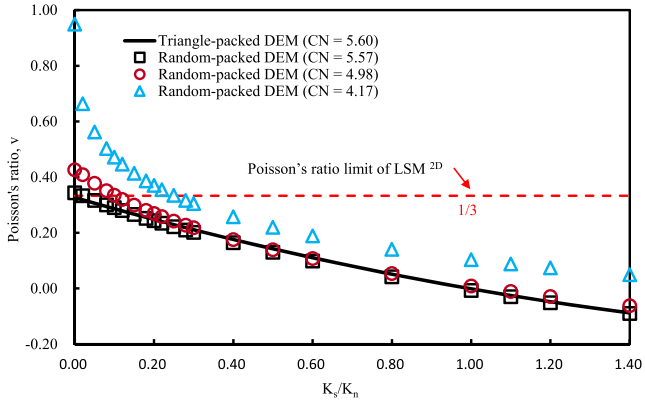

FIGURE 8 Relationship between the shear stiffness ratio and the Poisson's ratio of the random-packed DEM [Colour figure can be viewed at wileyonlinelibrary.com]

negative Poisson's ratio is obtained. It means the reductive effect of the shear stiffness on the Poisson's effect takes over that of the normal stiffness. In the work of Paster and Dyskin,[31] this phenomenon was experimentally demonstrated. When CN is small, the Poisson's effect is dominated by the geometric factor. Increase of the shear stiffness will not change the geometric distribution of the bonded particle model. Therefore, there is only one limit influence of the Poisson's ratio induced by the shear stiffness ratio compared with these models with larger CNs. Figure 9 shows the Young's modulus of the random-packed DEM. A similar trend as the triangle packed DEM is obtained. The influence of the shear stiffness ratio on the change of the elastic modulus is more appealing for DEM with smaller CN. Unlike in the triangle packed DEM, the *dWR* will influence slightly the Poisson's ratio (see Figure 10). It indicates that the moment transfer between particles has only a minor influence on the Poisson's ratio of the random-packed DEM. The shear stiffness ratio is set to zero to eliminate the influence of the shear spring.

The Poisson's ratios of models with various CN are plotted in Figure 11. When increasing the CN, the predicted Poisson's ratio decreases, while, there is a low bound value of 1/3. Considering Figures 8 and 11 together, it can be concluded that both mechanical and geometric factors are required in the bonded DEM to reproduce a full range of Poisson's ratios. For well-connected models, the represented Poisson's ratio of the bonded DEM can only be adjusted to values below 1/3. When Poisson's ratio is larger than 1/3, a geometric factor has to be introduced. The shear spring is a local factor (bond level), while the CN is a global factor (particle model level). When the bonded DEM is used to represent a plane stress condition, the represented Poisson's ratio must not be larger than 0.5. The reasons for the reproduced Poisson's ratio being larger than 0.5 will be explained in Section 3.3.1.

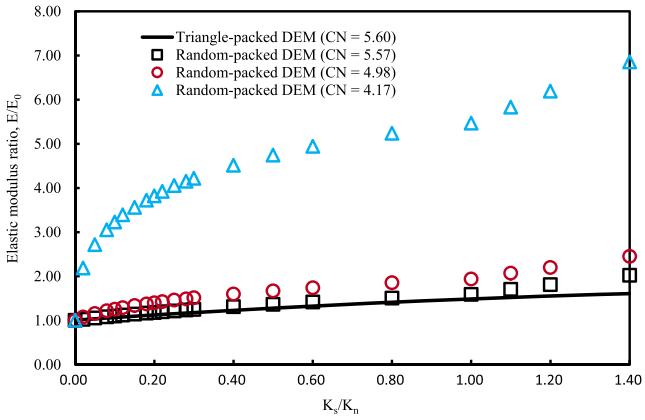

FIGURE 9 Influence of the shear stiffness ratio on the elastic modulus ratio of the random-packed DEM [Colour figure can be viewed at wileyonlinelibrary.com]

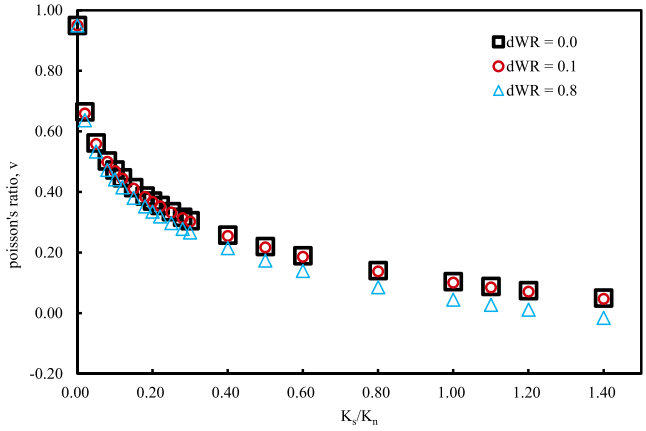

FIGURE 10 Influence of the bond thickness ratio on the Poisson's ratio of the random-packed DEM [Colour figure can be viewed at wileyonlinelibrary.com]

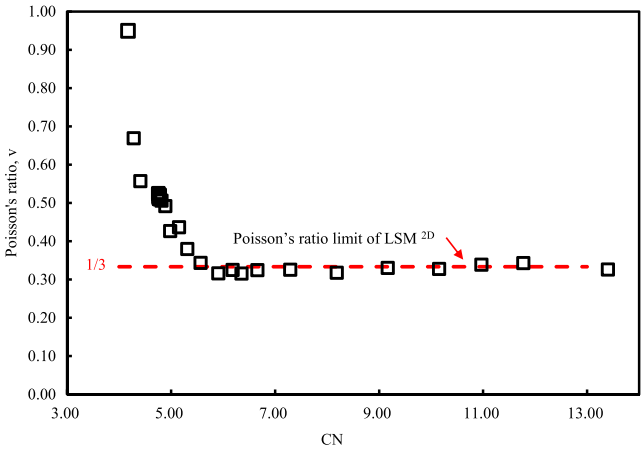

FIGURE 11 Relationship between CN and the Poisson's ratio of the random-packed DEM [Colour figure can be viewed at wileyonlinelibrary.com]

3.2.2 | Elastic problem with complex deformation field

The same random-packed particle model as in the previous section is used in the boundary value problem shown in Figure 12. The left and bottom sides of the model were fixed, while the top wall, which again does not extend across the entire top boundary, is moved by a velocity to impose a displacement of 0.1064 m and to get a static solution. Models with different CNs are considered. Figure 13 shows the simulation results of the bonded DEM and the plane stress FEM. It may be concluded that the random-packed DEM can give reasonable results for the elastic boundary value problem. The purpose of plotting results for models with different CNs is to show the multiple solution properties of stiffness parameters selection of the 2D bonded DEM. Unlike FEM, elastic modulus and Poisson's ratio are determined for a given problem, multiple solutions are existing for the bonded DEM representing the same elastic boundary value problems. By using particle models with different CNs to reproduce the same Poisson's ratios; each may reproduce a good fit with the FEM solution.

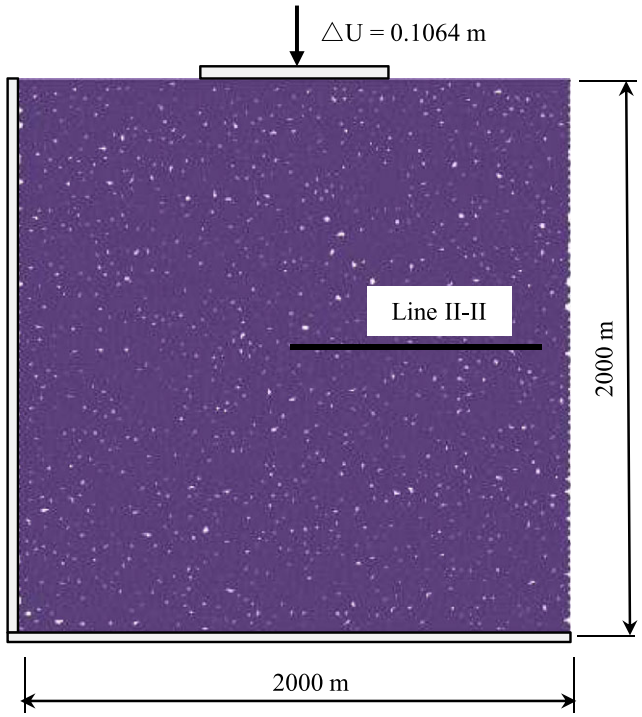

FIGURE 12 Computational model of the random-packed DEM for a boundary-value problem [Colour figure can be viewed at wileyonlinelibrary.com]

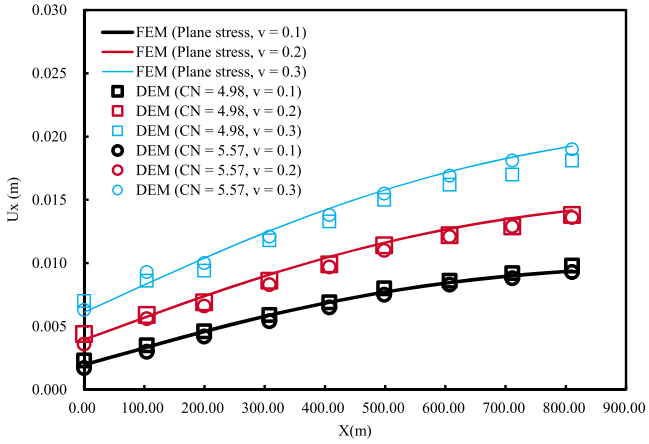

FIGURE 13 Quantitative comparison of displacements predicted by the plane stress FEM and the random-packed DEM [Colour figure can be viewed at wileyonlinelibrary.com]

3.3 | Hyper elasticity analysis and DLSM

3.3.1 | The Poisson's ratio

In this work, the Poisson's ratio obtained from Equation 29 is called as the apparent Poisson's ratio. When the 2D bonded DEM represents the plane stress problem, it equals to the Poisson's ratio of the target material. For a full 3D model, the corresponding calculation of Equation 29 also equals to the material's actual Poisson's value. However, when the 2D bond DEM is used to model a plane strain problem, a further convention is required to obtain the Poisson's ratio of the modeled material.

When the 2D bonded DEM is used to simulate the plane strain condition, the Poisson's ratio and Young's modulus calculated from Equations 29 and 30 should be further processed. According to the classical elasticity, the Poisson's ratio and Young's modulus of the target material (E' and v') should be obtained using the following equations:

$$v' = \frac{v}{1+v} \tag{31}$$

$$E' = \frac{E(1+2v)}{(1+v)^2} \tag{32}$$

where E and v are the corresponding values obtained from Equations 29 and 30.

The results shown in Figure 8 were further processed using Equation 31 and plotted in Figure 14 together with the analytical solution (Equation 23) derived from the hyper elasticity analysis. Good agreements can be observed between the analytical and numerical predictions of the 2D bonded DEM (with large CN). In Figure 14, the Poisson's ratios are all referring to the material parameters. Here, the 2D bonded DEM is viewed as plane strain condition. From Equation 31, it can be seen that the corresponding Poisson's ratio is actually 0.5 when the Poisson's ratio obtained via Equation 30 is 1.0. Therefore, the results shown in Figure 11 are still reasonable due to the plane strain nature of the bonded DEM in 2D. Under the plane strain condition, the corresponding calibrated elastic parameters of the 2D bonded DEM with Equations 29 and 30 should be further processed using Equations 31 and 32.

To further investigate the influence of the model's dimension, a full 3D numerical simulation is conducted by using the DLSM. The model size is 2000 m × 2000 m × 400 m, and the particle size is 20 m. The regular packing (Cubic-II)[18] is adopted. The boundary conditions are the same as those for the 2D bonded DEM except the out plane boundaries have been set free (to mimic the plane stress condition). The Poisson's ratio was directly obtained using Equation 29 and shown in Figure 14. It is found that the DLSM can go beyond the upper bound value of the Poisson's ratio represented by the bonded DEM even without help of the geometric factor (random packed particle model). The DLSM can reproduce stable solution despite the shear stiffness being negative (see Figure 14). The reason is the introduction of the multi-body shear spring in the DLSM. In DLSM, a negative shear stiffness refers the shape of potential variation

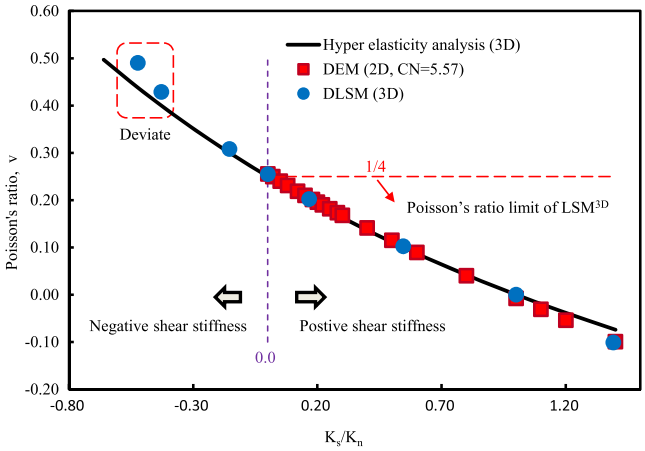

FIGURE 14 Comparison between the actual Poisson's ratio predicted by the 3D hyper elasticity analysis, the random-packed DEM2D, and the DLSM3D [Colour figure can be viewed at wileyonlinelibrary.com]

function due to shear deformation is downwards.[32] Details of the physical interpretation at the atomic scale can be found in the paper of Zhao et al.[32]

The results also show that the hyper elasticity analysis is able to study the elastic responses of the bonded DEM with random packed models with well-connected bonds (large CN). However, when the Poisson's ratio is close to 0.5, a deviation can be found (see Figure 14). This disagreement is not related to the particle rotation and homogenous deformation assumption (note: both the hyper elasticity analysis and DLSM are free of these influence) but caused by the discrete nature of the bonded DEM (note: the 2D bonded DEM and the DLSM possess the same behavior).

3.3.2 | Elastic problem with complex deformation field

In this section, an elastic problem is solved by the bonded DEM, the DLSM, and the plane strain FEM. The same boundary conditions as in the Section 3.2.2 are applied. In the 3D simulation with the DLSM, the same model as the uniaxial compressive test is adopted; the plane strain condition is implemented by fixing the deformation along the out-of-plane directions. For these simulations with the bonded DEM, the shear stiffness was set to zero. Different Poisson's ratios are obtained by varying CN. Figure 15 shows the simulated results of the DEM, the plane strain FEM, and the DLSM. When the Poisson's ratios are 0.24 and 0.34, good agreements between these models are observed. However, when the Poisson's ratio is close to 0.5, (ie, 0.49), the simulation results of the DEM and the DLSM are different from the

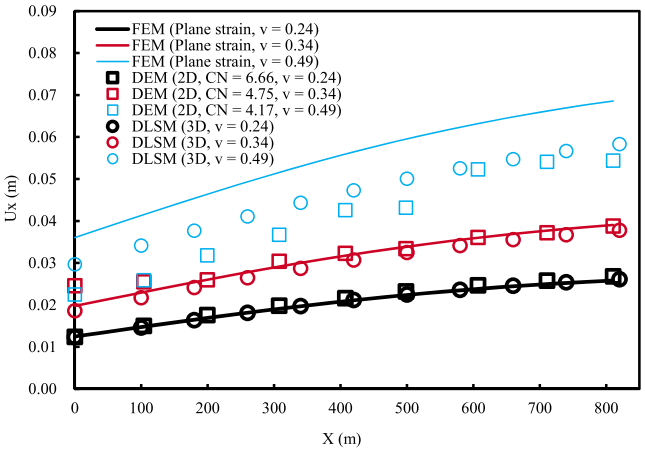

FIGURE 15 Quantitative comparison of displacements for the boundary value problem predicted by the plane strain FEM, the DEM2D, and the DLSM3D [Colour figure can be viewed at wileyonlinelibrary.com]

prediction of the plane strain FEM. Therefore, caution must be taken when discontinuum-based models (the bonded DEM and the DLSM) are used for elastic problems whose Poisson's ratio is close to 0.5. Additional experimental exploration is required to assess which method (continuum or discontinuum) is closer to the reality. It may be case dependent. Discontinuum-based models may be good for some materials while continuum-based ones better for others.

3.4 | Rock cutting by the bonded DEM

Figure 16A shows the computational model for a rock cutting problem. The adopted particle model is the same as that used for the problem shown in Figure 12. The boundary conditions are modified for the rock cutting problem. Three walls are used to fix the rock block. A cutter is placed on the left of the rock block with an inclination angle of 30°. During the simulation, the cutter is subjected to a velocity of 3 m/s. Two simulations are conducted using two different shear stiffness ratios ($K_s/K_n = 0.0$, $K_s/K_n = 0.2$), while all other parameters are kept the same. Figure 16B,C shows the simulated results, and completely different fracture patterns are observed. Different fracture length, fracture surface roughness, and fragmentation chip shapes are obtained. The variation of elastic modulus has little effect on the fracturing paths and fragmentation patterns. Therefore, it is concluded that the Poisson's ratio is the most important factor in fracturing and fragmentation simulation when using the bonded DEM. It highlights the importance of appropriate selection of elastic parameters for the 2D bonded DEM.

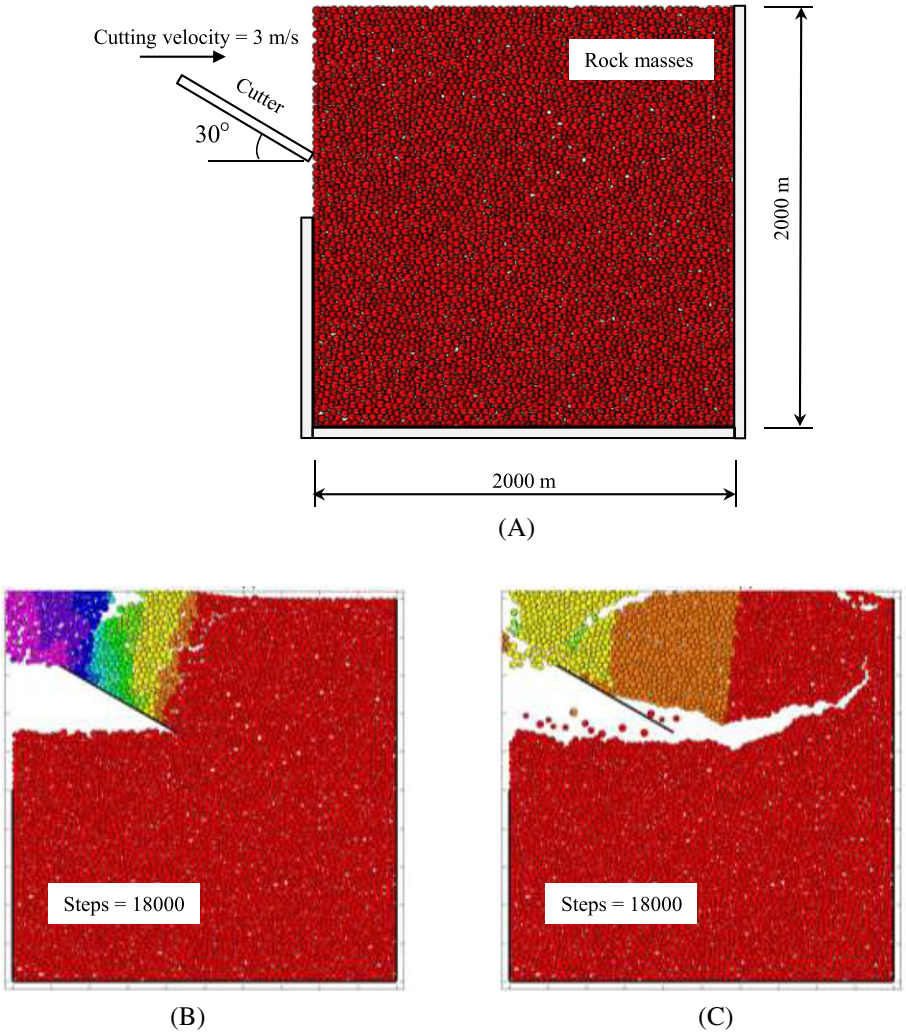

FIGURE 16 Simulation results on a rock cutting process using the bonded DEM with different shear stuffiness ratios (reproduced different Poisson's ratios): A, computational model; B, Ks/Kn = 0.0, $\nu = 0.34$; and C, Ks/Kn = 0.2, $\nu = 0.24$ [Colour figure can be viewed at wileyonlinelibrary.com]

4 | CONCLUSIONS

This work investigated the elastic responses of the 2D bonded DEM. Numerical results of both triangle-packed and random-packed models suggested that the particle rotation and moment transfer between particles are minor factors for elastic behavior of the 2D bonded DEM. We also found two dominant factors in the 2D bonded DEM, namely, the shear stiffness ratio and the average CN. A critical value of the Poisson's ratio at 1/3 (1/4 under 3D and plane strain conditions) exists for these two factors. By comparison with FEM outputs, we conclude that the 2D bonded DEM is capable of reproducing reasonable elastic deformation under both plane stress and plane strain conditions. However, elastic problems cannot be replicated reasonably when CN is significantly large (that is when long-range interaction is considered) or the Poisson's ratio approaches 1/2. Finally, a rock cutting simulation demonstrated that correctly selecting elastic parameters is crucial for the bonded DEM to rationally model fracturing, fragmentation, and failure of solids.

In summary, the key findings of this work are (1) to represent a full range of Poisson's ratios the 2D bonded DEM has to use both the non-central interaction (shear spring) and a random-packed particle model; (2) the 2D bonded DEM behaves according to classical elasticity rather than the micro-polar elasticity; (3) when long-range interaction is considered, the 2D bonded DEM may fail to predict correct displacement results of elastic boundary value problems; (4) the displacement prediction of the 2D bonded DEM deviates from the elastic solution when the represented Poisson's ratio is close to 0.5; and (5) the fracturing and fragmentation results of the 2D bonded DEM are highly influenced by the elastic parameters (especially the Poisson's ratio). These findings are important to have a more rational and confident application of the 2D bonded DEM to solve geotechnical problems.[33]

ACKNOWLEDGEMENTS

This research is financially supported by the National Natural Science Foundation of China (Grant No. 1177020290).

ORCID

Gao-Feng Zhao http://orcid.org/0000-0001-9962-8743

REFERENCES

1. Cundall PA. A computer model for simulating progressive, large-scale movements in block rock systems. *Symp Int Society Rock Mech*. 1971;1(ii-b):11-18.
2. Sibille L, Hadda N, Nicot F, Tordesillas A, Darve F. Granular plasticity, a contribution from discrete mechanics. *J Mech Phys Solids*. 2015;75:119-139.
3. Potyondy DO, Cundall PA. A bonded-particle model for rock. *Int J Rock Mech Min Sci*. 2004;41(8):1329-1364.
4. Maheo L, Dau F, André D, Charles JL, Iordanoff I. A promising way to model cracks in composite using discrete element method. *Compos Part B Eng*. 2015;71(71):193-202.
5. Hentz S, Daudeville L, Donzé FV. Discrete element modeling of a reinforced concrete structure. *J Mech Behav Mater*. 2009;19(4):249-258.
6. Zhang XP, Wong LNY. Crack initiation, propagation and coalescence in rock-like material containing two flaws: a numerical study based on bonded-particle model approach. *Rock Mech Rock Eng*. 2013;46(5):1001-1021.
7. Yang SQ, Huang YH, Jing HW, Liu XR. Discrete element modeling on fracture coalescence behavior of red sandstone containing two unparallel fissures under uniaxial compression. *Eng Geology*. 2014;178(6):28-48.
8. Li XF, Li HB, Liu YQ, Zhou QC, Xia X. Numerical simulation of rock fragmentation mechanisms subject to wedge penetration for TBM. *Tunnel under Space Tech*. 2016;53(5):96-108.
9. Oetomo JJ, Vincens E, Dedecker F, Morel JC. Modeling the 2d behavior of dry-stone retaining walls by a fully discrete element method. *Int J Numeri Analy Meth Geomech*. 2016;40(7):1099-1120.
10. Jiang M, Jiang T, Crosta GB, Shi Z, Chen H, Zhang N. Modeling failure of jointed rock slope with two main joint sets using a novel DEM bond contact model. *Eng Geology*. 2015;193:79-96.
11. Yoon JS, Zimmermann G, Zang A. Numerical investigation on stress shadowing in fluid injection-induced fracture propagation in naturally fractured geothermal reservoirs. *Rock Mech Rock Eng*. 2015;48(4):1439-1454.
12. Hughes AN, Benesh NP, Shaw JH. Factors that control the development of fault-bend versus fault-propagation folds: insights from mechanical models based on the discrete element method (DEM). *J Struct Geology*. 2014;68:121-141.

13. Schöpfer MPJ, Childs C, Manzocchi T. Three-dimensional failure envelopes and the brittle-ductile transition. *J Geophys Res*. 2013;118(4):1378-1392.
14. Hrennikoff A. Solution of problems of elasticity by the framework method. *ASME J Appl Mech*. 1941;8:A619-A715.
15. Mora P, Place D. A lattice solid model for the nonlinear dynamics of earthquakes. *Int J Mod Phys C*. 1993;4(06):1059-1074.
16. Gao HJ, Klein P. Numerical simulation of crack growth in an isotropic solid with randomized internal cohesive bond. *J Mech Phys Solids*. 1998;46(2):187-218.
17. Lilliu G, van Mier JGM. 3D lattice type fracture model for concrete. *Eng Fract Mech*. 2003;70(7-8):927-941.
18. Zhao G-F, Fang J, Zhao J. A 3d distinct lattice spring model for elasticity and dynamic failure. *Int J Numeri Analy Meth Geomech*. 2011;35(8):859-885.
19. Chen H, Lin E, Jiao Y, Liu Y. A generalized 2D non-local lattice spring model for fracture simulation. *Comput Mech*. 2014;54(6):1541-1558.
20. Zhang Z, Yao Y, Mao X. Modeling wave propagation induced fracture in rock with correlated lattice bond cell. *Int J Rock Mech Min Sci*. 2015;78:262-270.
21. Zhang Z, Chen Y. Modeling nonlinear elastic solid with correlated lattice bond cell for dynamic fracture simulation. *Comput Methods Appl Mech Eng*. 2014;279:325-347.
22. Zhao G-F. Developing a four-dimensional lattice spring model for mechanical responses of solids. *Comput Methods Appl Mech Eng*. 2017;315(1):881-895.
23. Yoon J. Application of experimental design and optimization to pfc model calibration in uniaxial compression simulation. *Int J Rock Mech Min Sci*. 2007;44(6):871-889.
24. Kazerani T, Zhao J. Micromechanical parameters in bonded particle method for modelling of brittle material failure. *Int J Numeri Analy Meth Geomech*. 2010;34(18):1877-1895.
25. Wang Y, Mora P. Macroscopic elastic properties of regular lattices. *J Mech Phys Solids*. 2008;56(12):3459-3474.
26. Hahn M, Wallmersperger T, Kröplin BH. Discrete element representation of continua: proof of concept and determination of the material parameters. *Comput Mater Sci*. 2010;50(2):391-402.
27. Azevedo NM, Lemos JV. A 3d generalized rigid particle contact model for rock fracture. *Eng Comput*. 2013;30(2):277-300.
28. Scholtès L, Donzé FV. A DEM model for soft and hard rocks: role of grain interlocking on strength. *J Mech Phys Solids*. 2013;61(2):352-369.
29. Zhao G-F. *High Performance Computing and the Discrete Element Model: Opportunity and Challenge*. UK: ISTE Press Ltd; 2015.
30. Zhang ZN, Ge XR. Micromechanical consideration of tensile crack behavior based on virtual internal bond in contrast to cohesive stress. *Theoret Appl Fract Mech*. 2005;43(3):342-359.
31. Pasternak E, Dyskin AV. Materials and structures with macroscopic negative poisson's ratio. *Int J Eng Sci*. 2012;52:103-114.
32. Zhao SF, Zhao GF. Implementation of a high order lattice spring model for elasticity. *Int J Solids Struct*. 2012;49(18):2568-2581.
33. Wu W, Zhao Z, Duan K. Unloading-induced instability of a simulated granular fault and implications for excavation-induced seismicity. *Tunnel Underg Space Tech*. 2017;63:154-161.

How to cite this article: Zhao G-F, Yin Q, Russell AR, Li Y, Wu W, Li Q. On the linear elastic responses of the 2D bonded discrete element model. *Int J Numer Anal Methods Geomech*. 2018;1–17. https://doi.org/10.1002/nag.2858